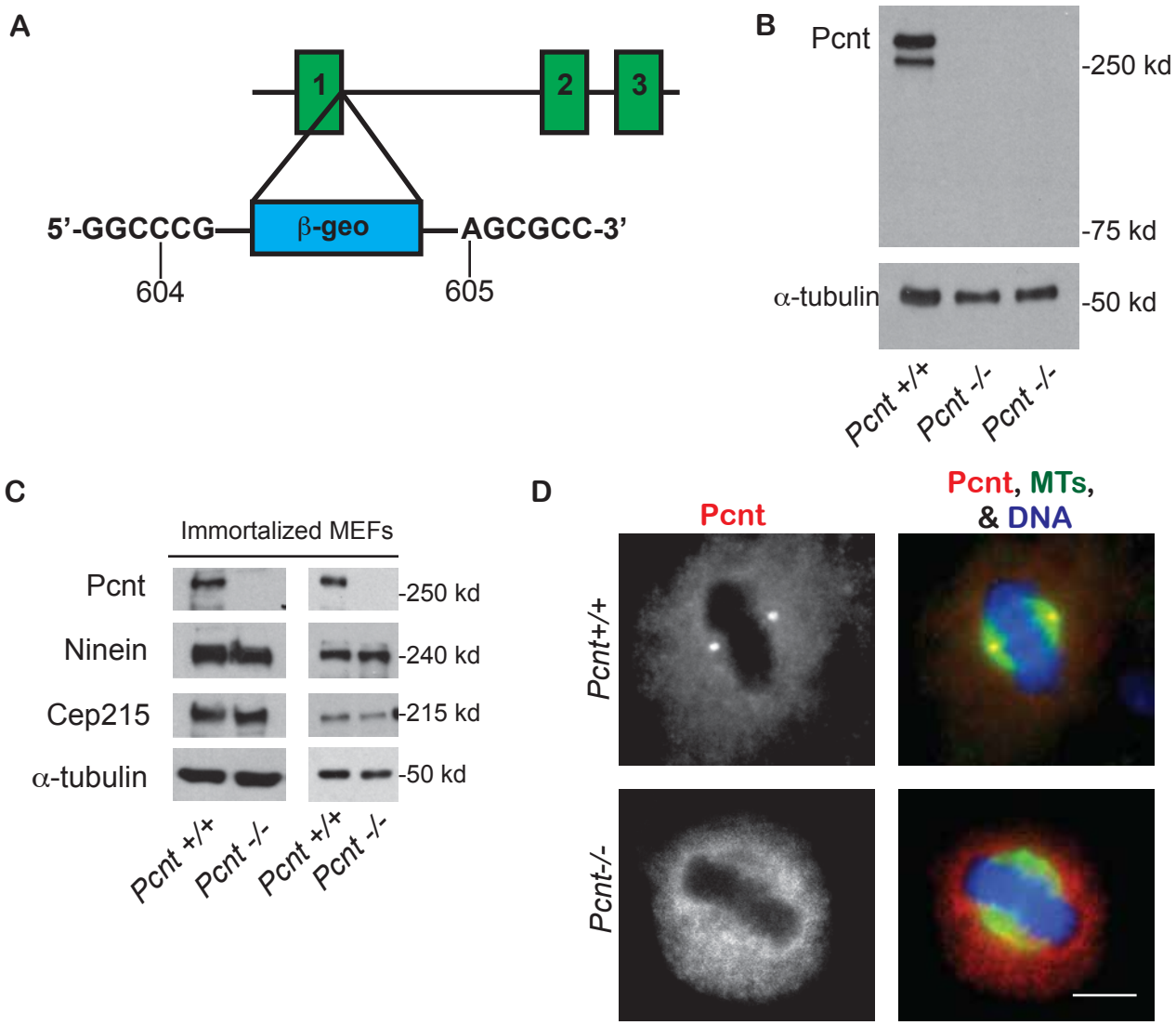
A
1
2
3
5'-GGCCCG
β-geo
AGCGCC-3'
604
605
B
Pcnt
-250 kd
-75 kd
α-tubulin
-50 kd
Pcnt +/+
Pcnt -/-
Pcnt -/-
C
Immortalized MEFs
Pcnt
Ninein
Cep215
α-tubulin
-250 kd
-240 kd
-215 kd
-50 kd
Pcnt +/+
Pcnt -/-
Pcnt +/+
Pcnt -/-
D
Pcnt
Pcnt, MTs, & DNA
Pcnt+/+
Pcnt-/-

**Figure S1.**

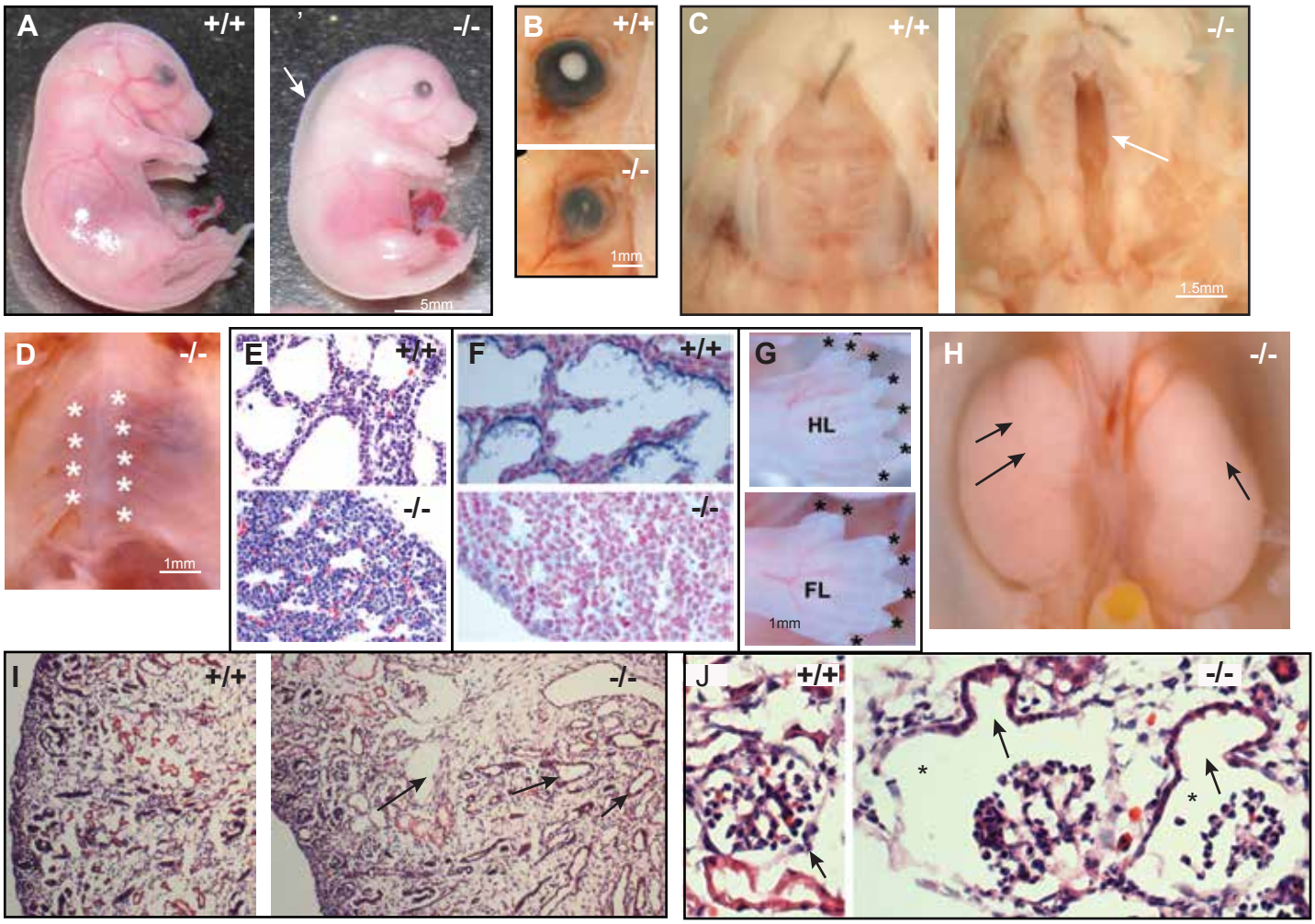


**Figure S2.**

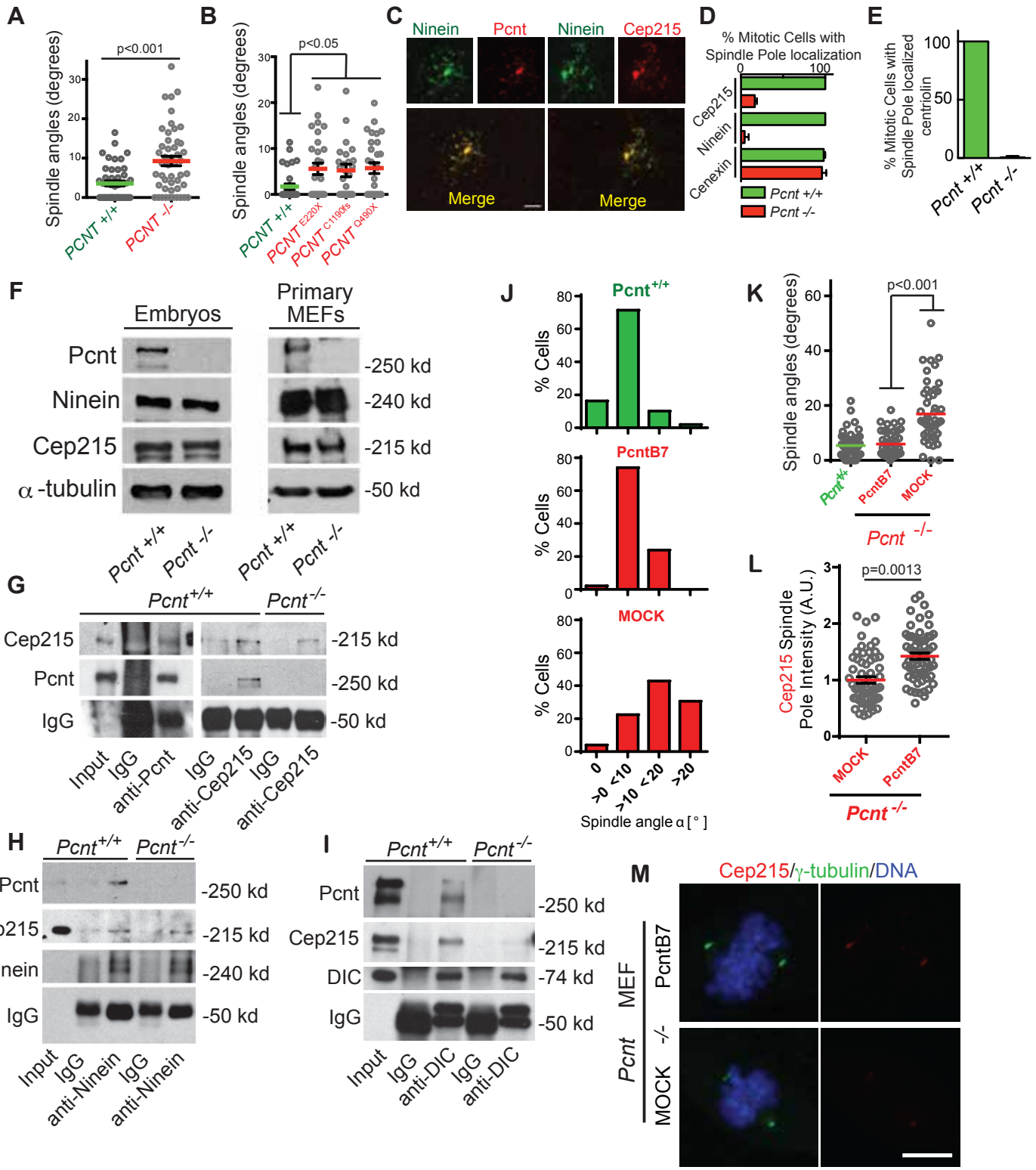
A
Spindle angles (degrees)
p<0.001
PCNT +/+
PCNT -/-
B
Spindle angles (degrees)
p<0.05
PCNT +/+
PCNT E220X
PCNT C1190fs
PCNT Q490X
C
Ninein
Pcnt
Ninein
Cep215
Merge
Merge
D
% Mitotic Cells with Spindle Pole localization
Cep215
Ninein
Cenexin
Pcnt +/+
Pcnt -/-
E
% Mitotic Cells with Spindle Pole localized centriolin
Pcnt +/+
Pcnt -/-
F
Embryos
Primary MEFs
Pcnt
Ninein
Cep215
α-tubulin
-250 kd
-240 kd
-215 kd
-50 kd
Pcnt +/+
Pcnt -/-
Pcnt +/+
Pcnt -/-
G
Pcnt+/+
Pcnt-/-
Cep215
Pcnt
IgG
-215 kd
-250 kd
-50 kd
Input
IgG
anti-Pcnt
IgG
anti-Cep215
IgG
anti-Cep215
H
Pcnt+/+
Pcnt-/-
Pcnt
Cep215
Ninein
IgG
-250 kd
-215 kd
-240 kd
-50 kd
Input
IgG
anti-Ninein
IgG
anti-Ninein
I
Pcnt+/+
Pcnt-/-
Pcnt
Cep215
DIC
IgG
-250 kd
-215 kd
-74 kd
-50 kd
Input
IgG
anti-DIC
IgG
anti-DIC
J
Pcnt+/+
PcntB7
MOCK
% Cells
0
>0
<10
>10
<20
>20
Spindle angle α [°]
K
Spindle angles (degrees)
p<0.001
Pcnt+/+
PcntB7
MOCK
Pcnt -/-
L
Cep215 Spindle Pole Intensity (A.U.)
p=0.0013
MOCK
PcntB7
Pcnt -/-
M
Cep215/γ-tubulin/DNA
Pcnt -/- MEF
PcntB7
MOCK

**Figure S3.**

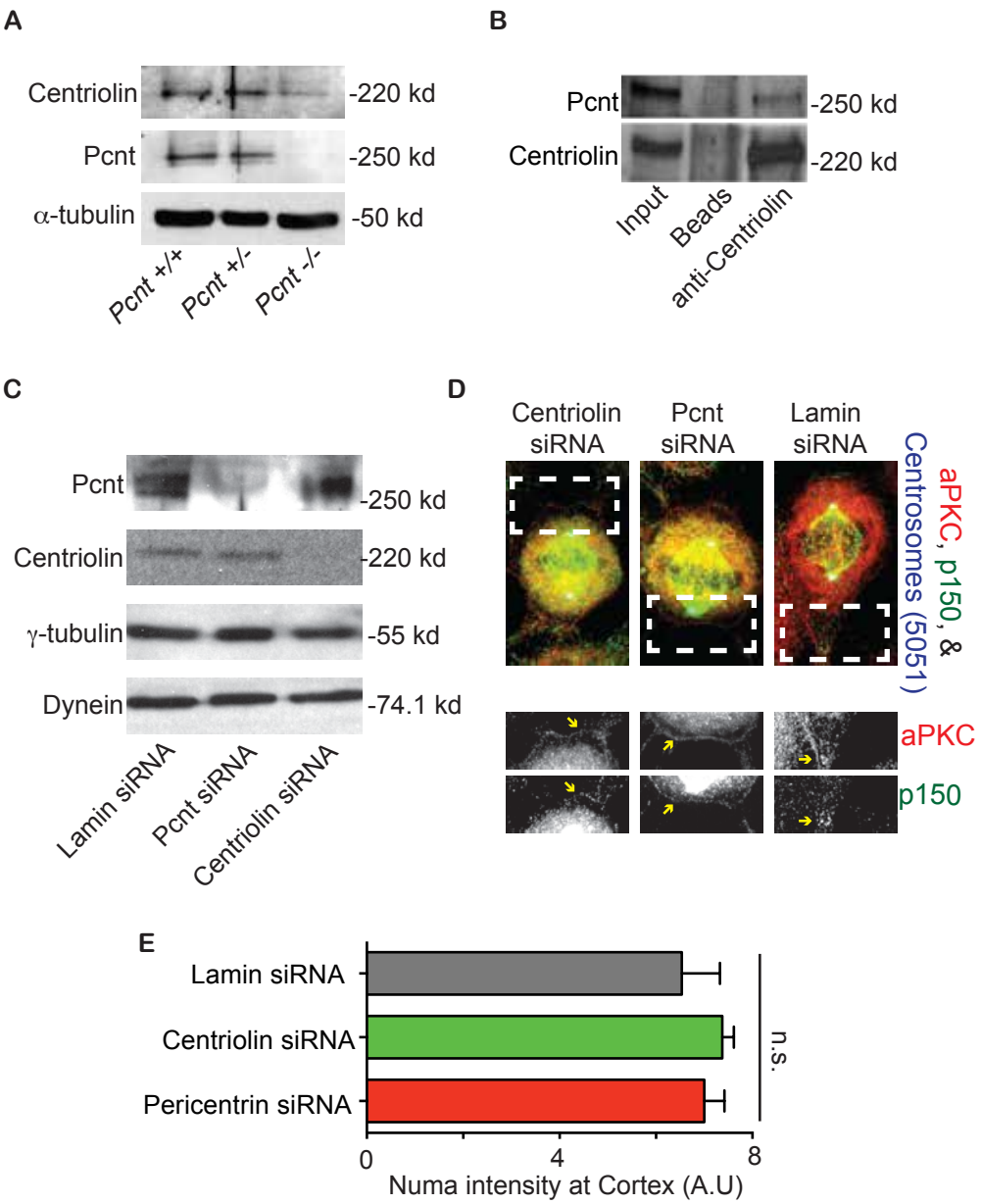
A
Centriolin
-220 kd
Pcnt
-250 kd
α-tubulin
-50 kd
Pcnt +/+
Pcnt +/-
Pcnt -/-
B
Pcnt
-250 kd
Centriolin
-220 kd
Input
Beads
anti-Centriolin
C
Pcnt
-250 kd
Centriolin
-220 kd
γ-tubulin
-55 kd
Dynein
-74.1 kd
Lamin siRNA
Pcnt siRNA
Centriolin siRNA
D
Centriolin siRNA
Pcnt siRNA
Lamin siRNA
aPKC, p150, & Centrosomes (5051)
aPKC
p150
E
Lamin siRNA
Centriolin siRNA
Pericentrin siRNA
n.s.
0
4
8
Numa intensity at Cortex (A.U)

**Figure S4.**

**Supplemental Data**

**Figure S1** (related to Fig. 1). **Disruption of mouse *Pcnt* allele by gene trap. (A)** Site of plasmid insertion of gene trap (β-geo). **(B,C)** Immunoblots showing Pcnt loss in the lysates from whole embryos **(B)** and immortalized MEFs **(C)**. **(D)** Immunofluorescence of $Pcnt^{-/-}$ and $Pcnt^{+/+}$ MEFs. No Pcnt was detected at spindle poles (left). Merged (right): Pcnt, red; microtubules (MTs), green; chromosomes (DNA), blue; Scale bar, 5μm.

**Figure S2** (related to Fig. 1). **Secondary phenotypes associated with $Pcnt^{-/-}$ mice.** $Pcnt^{-/-}$ and $Pcnt^{+/+}$ depicted as (+/+ or -/-). **(A)** Hydrops (A', arrow). **(B)** Microphthalmia. **(C)** Cleft palate (arrow). **(D)** Misaligned sternum ribs (*), right and left side of sternum. **(E)** Lung atelectasis. **(F)** Lack of lung surfactant (**F**, dark blue); nuclei, red. **(G)** Polydactyly (*), hindlimb (HL) and forelimb (FL). **(H)** Duplicated kidney (arrows). **(I)** Cystic kidney (arrow). **(J)** Glomerular and ductal cysts (*, arrows, respectively). Matched images, same magnification. These phenotypes occur in 50-100% of $Pcnt^{-/-}$ embryos.

**Figure S3** (related to Figure 2-3). **Characterization of spindle misorienatation and rescue of spindle angles. (A)** Quantification of spindle angles in Figure 2A for $Pcnt^{-/-}$ and $Pcnt^{+/+}$ MEFs ($p<0.001$). **(B)** A significant increase in misoriented spindles is observed in Pcnt-deficient MOPDII fibroblasts (red; $PCNT^{Q490X}$, $PCNT^{E220X}$, and $PCNT^{C1190fs}$; refer to Figure 2E-F) versus control human fibroblasts (green; *PCNT* +/+). 29-32 spindles were analyzed for each group. Individual angles represented in scatter plot. **(C)** Immunofluorescence of $Pcnt^{+/+}$ MEFs show partial co-localization of ninein (green) and Cep215 (red) to Pcnt-containing pericentriolar satellites (red). Bar, 2 μm. **(D)** Quantification demonstrates a significant decrease of Cep215 and ninein from mitotic spindle poles in $Pcnt^{-/-}$ cells (n=3 experiments, >150 mitotic cells/genotype, corresponds

to Figure 3A). **(E)** Quantification demonstrates a significant decrease of centriolin from mitotic spindle poles in *Pcnt*$^{-/-}$ cells (n=3 experiments, >150 mitotic cells/genotype, corresponds to Figure 3D). **(F)** Immunoblot of ninein and Cep215 from lysates of embryos and primary MEFs. Note that global levels of ninein and Cep215 remain constant between *Pcnt*$^{-/-}$ and *Pcnt*$^{+/+}$ littermates. Loading control, $\alpha$-tubulin. **(G-H)** Reciprocal immunoprecipitation confirmed the interactions between Pcnt, Cep215, and Ninein in *Pcnt*$^{+/+}$ MEFs (see in Figure 3B). **(I)** Loss of spindle pole proteins Pcnt, Ninein, and Cep215 was quantified in Pcnt- or Ninein-depleted cells and compared to control (Lamin siRNA; 30 spindle poles per treatment, representative of three experiments, *** depicts $p<0.001$, n.s. is non-significant). A significant loss of Ninein and Cep215 was observed with Pcnt-depletion, but neither Pcnt nor Cep215 were affected with Ninein-depletion. **(J-M)** Spindle misorientation was rescued with the expression of PcntB7 domain in *Pcnt*$^{-/-}$ MEFs (**J**; individual angles represented in **K;** 46-49 cells per group analyzed in three experiments, **** depicts $p<0.001$). Note that PcntB7 domain significantly increased Cep215 staining at spindle poles in *Pcnt*$^{-/-}$ MEFs (60-66 spindle poles analyzed in three experiments, $p=0.0013$; representative images are shown in **M**), suggesting a correlation between complex anchoring at the poles and spindle orientation.

**Figure S4** (related to Figure 3). **Centriolin interacts with Pcnt, and does not affect NuMA, p150$^{Glued}$ and aPKC localization. (A)** Immunoblot shows decreased centriolin levels in *Pcnt*$^{-/-}$, but not *Pcnt*$^{+/+}$ or *Pcnt*$^{+/-}$ MEFs. $\alpha$-tubulin, loading control. **(B)** Immunoprecipitation from human epithelial cells demonstrates an interaction between Pcnt and centriolin. **(C)** Immunoblot demonstrates centriolin and Pcnt-depletion using

previously published siRNAs [S1, S2]. **(D)** Centriolin-depleted cells showed decreased number and length of astral microtubules compared to control ($n > 50$ asters per treatment, $p < 0.001$). **(E)** Depletion of centriolin or Pcnt shows no adverse effects on two spindle orientation proteins, $p150^{glued}$ (green) and aPKC (red), during mitosis when compared to lamin siRNA control. Insets demonstrate localization of aPKC and p150 at cortex (yellow arrows). Centrosome labeled with anti-5051 (blue). **(F)** Quantification for NuMA at cortex in cells treated with Lamin, Pcnt, or Centriolin siRNAs shown (n=25 cells for each treatment, no significant difference between treatments.)

**Table S1** (related to Fig. 2)**. Summary of nine *Pcnt*$^{-/-}$ fetuses$^{\dagger}$ with cardiac defects and other types of anomalies**

| Fetus ID | Age | Echo Findings | Cardiovascular Defect | Histopathology | Lung | Kidney | Limb Defect | Eye | Others |
|---|---|---|---|---|---|---|---|---|---|
| P417-1 | E17.5 | Hydrops, enlarged LV with MR and AR, reversed DV a-flow | Severe hydrops with vasculature malformations seen on body surface, symmetric and duplicated carotid | DORV + AVSD (large primum ASD and inlet VSD +common AV valve) + multiple mVSDs | Hypoplasia | Abnormal kidney position | LFL-122345; LHL,RFL-112345; RHL-12345 with broaden thumb | No left eye, small right eye | cleft palate, small thymus |
| P414-1 | E17.5 | Regurgitant aortic flow at both E15.5 and E17.5 | Symmetric carotid, congested atria | Transitional AVSD (large primum ASD + small inlet VSD) | Hypoplasia | Cystic duplex kidneys | LFL, RFL-1122345; RHL-1112345; LHL-112345 | Small left eye, en-opthalmia right eye | Misaligned sternum, cleft palate, small thymus |
| P414-2 | E17.5 | MR at E15.5 without AR, AR seen at E17.5 | Congested heart with enlarged LV/RV, duplicated right carotid | Partial AVSD (primum ASD cleft MV)+ Multiple mVSDs | Hypoplasia | Cystic duplex kidneys | LFL, RFL-1122345; LHL, RHL-112345 | Small right eye | Misaligned sternum, cleft palate, small thymus |
| P434-1 | E17.5 | DAo forward flow at E11.5 and E13.5. MR+AR at E15.5 | Right sided aortic arch with symmetric carotid arteries. Congested heart with enlarged ventricles | primum ASD + muscular VSD, DORV+RAA | Hypoplasia | Cystic duplex kidneys | RFL-122345; LFL-112345; LHL, RHL-112345 | Micro-pthalmia/ En-opthalmia both eyes | Small deep recessed eyes, small thymus |
| P423-NA | Neo-nate | DAo forward flow at E11.5 and E13.5. Some AR at E17.5 | Symmetric carotid, congested atria with enlarged LV/RV | DORV + AVSD (large primum ASD and inlet VSD +common AV valve) + mVSD | Hypoplasia | Cystic enlarged duplex kidneys | LFL, RFL-1122345; LHL-112345; RHL-22345 | No right eye, small left eye | Abnormal rib, cleft palate, cystic pancreas |
| P422-NA | Neo-nate | Not ultrasound scanned | Heart congestion enlarged/hypertrophic right ventricle | Transitional AVSD (large primum ASD + small inlet VSD) | Hypoplasia | Enlarged bilateral duplex kidneys | RFL-112345; LFL-1122345; RHL, LHL - 112345 | No eyes | Abnormal rib, misaligned sternum |
| P422-NB | Neo-nate | Right side arch, abnorm ductus venosus flow at E15.5 and E17.5 | Right sided aortic arch (retroesophageal) with symmetrical caroid arteries. Heart congestion with enlarged ventricles | primum ASD + muscular VSD | Hypoplasia | Enlarged bilateral duplex kidneys | RFL-112345; LFL-112345; RHL, LHL - 112345 | No left eye, small right eye, | Cleft palate, abnormal hypoplastic gonad |
| P422-NC | Neo-nate | Not ultrasound scanned | Right sided aortic arch with symmetrical carotid arteries. Heart congestion with enlarged ventricles | primum ASD + muscular VSD | Hypoplasia | Duplex left kidney, small right kidney | RFL-1122345; LFL,LHL-112345; RHL-12345 with broaden thumb | No right eye, small left eye | Abnormal rib, cleft palate, abnormal liver situs |
| E72 | E17.5 | Not ultrasound scanned | Enlarged and congested atria, SVC and IVC, hypertrophic ventricles | AVSD (large primum ASD and inlet VSD +common AV valve) | Hypoplasia | Cystic enlarged bilateral duplex kidneys, | LFL-112345; RFL-1122345; LHL-112345 | Small - Both eyes | Abnormal body curvature, small white spleen |

Shaded samples are those that have been ultrasound scanned and found to have abnormal cardiovascular function.

A : aortic regurgitation, ASD: atrial septal defect, AV: atrioventricular, AVSD: atrioventricular septal defect, DAo: descending aorta, DORV: double outlet right ventricle, DV a-flow: ductus venosus atrial contraction associated flow, LFL: left hindlimb, RFL: right forelimb, LHL: left hindlimb RHL: right hindlimb (numbers indicate digit identity, with duplicated numbers indicating syndactyly with fusion of adjacent digits), LV: left ventricle, mVSD: muscular VSD, RAA: right sided aortic arch, RV: right ventricle MR: mitral valve regurgitation, VSD: ventricular septal defect.

## Supplemental Experimental Procedures

### Generation of *Pcnt* gene trap mice

We obtained a BayGenomics (BayGenomics Consortium, San Francisco, CA (Medline PMID: 12520002)) mouse embryonic stem cell (ESC) line RRU388, which carries a *Pcnt* allele disrupted by the insertion of a gene trap vector (pGT0Lxf). pGT0Lxf carries a splice-acceptor sequence upstream of the reporter gene, *β-geo* (a fusion gene of β-galactosidase and neomycin phosphotransferase II). Injection of these 129P2/OlaHsd cells into C57BL/6 blastocysts at the University of Massachusetts Medical School Transgenic Animal Modeling Core resulted in chimeric mice that were bred with C57BL/6 mice to obtain germline transmission of the *Pcnt* mutant allele. *Pcnt* mutant mice were backcrossed to C57BL/6 mice for 10 generations to generate a C57BL/6 line carrying the *Pcnt* mutation.

### Vector insertion site and genotyping

The 5' insertion site of pGT0Lxf into the *Pcnt* gene was verified and the 3' insertion site was determined using a series long range PCR approach. The 3' insertion site was successfully amplified from heterozygous DNA by PCR using a forward primer from the 3' end of the vector and a reverse primer from intron 1. Primer sequences were: forward, 5'-TTCCCCGAAAAGTGCCACC-3' and reverse, 5'-TGAGGCAGAAGGAGGTGAGAAGAG-3'. The PCR product was cloned into the pCR 2.1-TOPO vector (Invitrogen, Carlsbad, CA) and amplified for sequencing.

A PCR genotyping strategy differentiates between the mutant and wild-type alleles. A common forward primer was used in combination with reverse primers specific to each

allele. Primer sequences were: forward, 5'-CGGTGGGGAAGAAATCCTAAAGC-3'; mutant reverse, 5'-TAGGACAAGAGGGCGAGACCAC-3'; and wild-type reverse, 5'-CGGAAGCACAACAACTAAGAATGC-3'. There primers amplified bands of 389 bp and 277 bp for the mutant and wild-type allele, respectively.

**Human and mouse cell cultures**

All human study subjects were obtained with approval either by the University of Texas Southwestern Medical Center Institutional Review Board or as described in [S3]. Skin fibroblast cultures were established from three unrelated subjects with primordial dwarfism. Control adult human dermal fibroblasts were obtained from ATCC (Manassas, VA). All cell lines were prepared from fresh skin biopsies, were not transformed and used at low passage number. This strategy was followed to avoid mitotic defects that occur during transformation and long-term passage.

Mouse embryonic fibroblasts (MEFs) were isolated following the protocol provided by Stephen Jones (Director, Transgenic/Knockout Mouse Core, UMASS Medical School). Briefly, a timed pregnant female was sacrificed at embryonic day 13.5. Under sterile conditions, embryos were dissected from their placenta and surrounding membranes, and their organs and head removed. Fibroblasts were isolated by repeated trypsinization of minced tissue (0.04% Trypsin in DMEM). Cells were grown in DMEM, 10% FBS, and penicillin/streptomycin at 37˚ C, and used for immunofluorescence analysis at passage 3 or lower. Immortalized MEF lines were established following standard procedures [S4].

**Histological analysis**

Mouse embryos were sacrificed at the indicated embryonic day; selected tissues and organs were removed, fixed in 4% paraformaldehyde (PFA) at 4˚C, and embedded in paraffin. For frozen sections, after fixation tissues or organs were cryoprotected in 30% sucrose at 4˚C until equilibrated, and then frozen in OCT compound. Samples were sectioned at 5-10 μm, mounted onto slides, and subjected to H&E or Thionin (Nissl) staining.

**Mouse Doppler echocardiography and cardiac histopathology analysis**

Ultrasound scanning of the cardiovascular system was initiated from embryonic day 11.5 to 17.5 using a VisualSonics Vevo 2100 Imaging System (VisualSonic, Inc, Toronto, ON, Canada) equipped with a 30-MHz phased linear array transducer. The mother was sedated using 1.5% isofluorane, with her body temperature maintained at 36-37°C, and heart rate at 450-550 beats per minute (bpm). The resolution was 50μm axial, 110μm lateral, and temporal frame rate in B-mode was set at 250 to 500 Hz maxima, and with a 0.15 mm sampling gate used to obtain blood flow velocities. The spectral Doppler images were recorded in multiple screen shots, with the Doppler measurements obtained from the mean of 3 cardiac cycles. To minimize Doppler velocity error, we only included spectral Doppler tracings where Doppler incident angles were less than 50 degrees. Color Doppler imaging was performed to obtain the flow velocities and time intervals from spectral Doppler to assess fetal hemodynamic function.

After ultrasound scanning, the embryos were necropsied and fixed in 10% formalin. To ensure the hearts arrested at diastole, prior to fixation, the embryos were perfused with potassium chloride. Standard histopathological analysis by episcopic fluorescence image capture (EFIC) was carried out as previously described [S5]. EFIC imaging was used to generate 3D reconstructions for examining the internal anatomy of the heart.

**Immunohistochemistry and immunofluorescence**

*Whole-mount PECAM immunohistochemistry* The procedure was performed as previously described [S6]. Briefly, embryos at embryonic day 11.5 were fixed in 4% PFA at 4˚C overnight, dehydrated and then rehydrated in graded methanol. After incubation in PBS with 0.5% Triton X-100 and treatment of proteinase K (20 μg/μl), samples were stained with anti-CD31 antibody (1:150) at 4˚C for overnight, followed by incubation of biotinylated secondary antibody, VECTASTAIN elite ABC kit and ImmPACT DAB. Vascular densities delineated by PECAM labeling were assessed by counting the number of vascular networks in different areas of the embryos using Openlab imaging software (PerkinElmer, Waltham MA).

*Immunohistochemistry on tissue sections* Embryonic and neonate tissues were immersion-fixed in 4% phosphate-buffered PFA, processed for paraffin embedding, and cut into 4-8 μm sections. Sections were deparaffinized, rehydrated and incubated with anti-NeuN, anti-TUJ1 and anti-MAP2 antibodies (brain); anti-surfactant antibodies (lung); other antibodies appropriate for detection of centrosome and microtubules (see Antibodies, Supplementary Information). Immunoreactivity was visualized with ABC kits (Vector Labs, Burlingame, CA), using diaminobenzidine (DAB) or BCIP/NBT as

chromogens. Retrievagen A (pH 6.0; BD Biosciences, San Jose, CA) was used for antigen retrieval after dewaxing when needed.

*Immunofluorescence* Staining procedures for cultured cells were performed as previously described [S7]. Cryosections were post-fixed with acetone for 30min, incubated with blocking buffer (PBS with 0.5% Triton X-100, 5% goat serum, and 1% bovine serum albumin) for 1 hour, and stained with primary and secondary antibodies for overnight at 4˚C.

**Spindle orientation assay**

Determination of spindle orientation relative to the horizontal plane or ventricular surface was performed as previously described [S8]. Briefly, spindle angle was estimated using inverse trigonometric functions, specifically, Arctan [S7]. Thus, if two spindle poles are in focus at the same z-plane, the estimated spindle orientation would be 0 (degree). For cultured cells, at least 30 mitotic spindles were scored for each category in each experiment. For asymmetric divisions in the ventricular zone of the brain, a total of 16-20 tissue samples were analyzed per mouse. For each tissue sample, data were collected as a Z-series image stack with depths of 6-10 μm (0.2 μm per step) and three image stacks were made. This allowed complete imaging of the ventricular zone and comparison with equivalent sections from wild-type littermates.

**Immunoblotting and immunoprecipitation**

Embryonic tissues and cultured cells were homogenized and lysed in lysis buffer (50mM Hepes (pH 7.5), 150mM NaCl, 1.5mM $MgCl_2$, 1 mM EGTA, 1% IGEPAL CA-630, and protease inhibitors (Complete Mini, Roche Diagnostics, Mannheim, Germany)). Clarified

lysates were used for immunoblotting and immunoprecipitation, following procedures previously described [8]. Of note, 200-500 μg of lysate were used per immunoprecipitation, and were precleared with either Protein G PLUS-Agarose beads (Santa Cruz Biotechnology, Dallas, TX) or TrueBlot beads (Rockland Immunochemicals Inc., Gibertsville, PA).

**Microscopy**

Images of cells or tissue sections were taken using either a Zeiss Axioskop2, PlanFLUOR 1.3 NA 100x lens and a Hamamatsu Orca camera or a Zeiss Axiovert 200 with a PerkinElmer UltraView spinning disk confocal, PlanAPO 1.4 NA 100x lens, and a Hammamatsu Orca camera. Fluorescence intensity measurements and scaling of images were carried out using Metamorph (Molecular Devices, Downingtown, PA) or ImageJ software.

**Statistical analysis**

Statistics were performed using paired Student's t-test or unpaired with Welch's correction, or Mann-Whitney U-test, for two-group comparison. When comparing more groups is required due to experimental design, Kruskal-Wallis test with *ad hoc* multiple comparisons is employed, as appropriate. *p* values less than 0.05 were considered statistically significant.

**RT-PCR for mRNA expression of *Pcnt***

Total RNA was extracted from embryo tissue using TRIzol reagent (Invitrogen, Carlsbad, CA). RNA was used as a template for cDNA synthesis using the One-Step RT-PCR kit

(Qiagen, Valencia, CA) as recommended by the manufacturer. Primer sequences were: *Pcnt* forward, 5'-GGAGTGTAAATAGAGCGAAGGCG-3'; *Pcnt* reverse, 5'-GCAGGTCAGTCACATCCAGTTCAC-3'. β-actin forward, 5'-GTGGGCCGCTCTAGGCACCAA-3'; reverse, 5'-CTCTTTGATGTCACGCACGATTTC-3'. These primers amplified bands of 380 bp and 540 bp for *pericentrin* and β-actin, respectively.

**siRNAs**

Previously characterized siRNAs targeting Pcnt, centriolin, and Lamin A/C were used as described [S1, S2]. Cells were examined 24–48 hours after siRNA treatment. siRNAs were used at 10–50 nM and delivered by Lipofectamine 2000 (Invitrogen) or HiPerfect (Qiagen) to Hela cells cultured in D-MEM supplemented with 5% fetal calf serum.

**Rescue of spindle misorientation with domain of Pcnt**

PcntB7 (Buchmann et al., 2007) was delivered to *Pcnt*$^{-/-}$ MEFs using Ingenio electroporation kit and Amaxa II nucleofector, and following manufacturer's procedures. *Pcnt*$^{-/-}$ and *Pcnt*$^{+/+}$ MEFs were fixed 48-72 hours after electroporation, and analyzed for spindle angles. Cells were also stained to detect desired proteins.

**Antibodies**

The following primary antibodies were used for immunostaining or biochemical assays: rabbit anti-pericentrin (ab4448, Abcam), rabbit anti-pericentrin (M8, Doxsey lab) [S9], mouse anti-pericentrin (611815, BD Biosciences), rabbit anti-CDK5RAP2/Cep215 (ABE236, EMD Millipore), rabbit anti-Centriolin (R2, Doxsey lab), rabbit anti-Cep215

(IHC-00063; Bethyl Laboratories), mouse anti-dynein intermediate chain (sc-13524: Santa Cruz Biotechnology), rabbit anti-Ninein (NB100-74631, Novus Biologicals), rabbit anti-Ninein (ab4447, Abcam), mouse anti-Ninein (gift of Gordon Chan lab), anti-NuMA (ab36999, Abcam), mouse anti-p150 (P50520-050, BD Biosciences), mouse anti-centrin (20H5, gift of Salisbury; 04-1624, EMD Millipore), rabbit anti-hCenexin1 (gift of Kyung Lee) [S10], rabbit anti-ODF2 (12058-1-AP, Protein Tech Group), rabbit anti-Cenexin/ODF2 (ab43840, Abcam), mouse anti-γ-tubulin(GTU-88, Sigma), rabbit anti-γ-tubulin (AATR, Doxsey lab), mouse anti-α-tubulin (DM1α, Sigma), rabbit anti-phospho-Histone H3 (Ser 10; 06-570, EMD Millipore), rabbit anti-surfactant (20R-SR011, Fitzgerald Industries, Concord, MA), rat anti-CD31 (NB600-1475, BD Biosciences).

Corresponding secondary antibodies for immunofluorescence were conjugated with Alexa 568 (Invitrogen, Carlsbad, CA); with Alexa 488, Alexa 647, Cy3, Cy5, DyLight 488 or DyLight 568 (Jackson ImmunoResearch, West Grove, PA). For immunoblotting, horseradish peroxidase (HRP) linked anti-mouse and anti-rabbit secondary antibodies (Jackson ImmunoResearch) were used.

**Supplemental References**


S1. Mikule, K., Delaval, B., Kaldis, P., Jurcyzk, A., Hergert, P., and Doxsey, S. (2007). Loss of centrosome integrity induces p38-p53-p21-dependent G1-S arrest. Nat. Cell Biol. *9*, 160–70.

S2. Hehnly, H., Chen, C.-T., Powers, C. M., Liu, H.-L., and Doxsey, S. (2012). The centrosome regulates the rab11- dependent recycling endosome pathway at appendages of the mother centriole. Curr. Biol. *22*, 1944–50.

S3. Griffith, E., Walker, S., Martin, C.-A., Vagnarelli, P., Stiff, T., Vernay, B., Al Sanna, N., Saggar, A., Hamel, B., Earnshaw, W. C., et al. (2008). Mutations in pericentrin cause Seckel syndrome with defective ATR-dependent DNA damage signaling. Nat. Genet. *40*, 232–6.

S4. Chen, J. J., Hong, Y., and Androphy, E. J. (1997). Mutational analysis of transcriptional activation by the bovine papillomavirus type 1 E6. Virology *236*, 30–6.

S5. Frank, L. H., Yu, Q., Francis, R., Tian, X., Samtani, R., Sahn, D. J., Leatherbury, L., and Lo, C. W. (2010). Ventricular rotation is independent of cardiac looping: a study in mice with situs inversus totalis using speckle-tracking echocardiography. J. Am. Soc. Echocardiogr. *23*, 315–23.

S6. Rhee, D. Y., Zhao, X.-Q., Francis, R. J. B., Huang, G. Y., Mably, J. D., and Lo, C. W. (2009). Connexin 43 regulates epicardial cell polarity and migration in coronary vascular development. Development *136*, 3185–93.

S7. Kuo, T.-C., Chen, C.-T., Baron, D., Onder, T. T., Loewer, S., Almeida, S., Weismann, C. M., Xu, P., Houghton, J.-M., Gao, F.-B., et al. (2011). Midbody accumulation through evasion of autophagy contributes to cellular reprogramming and tumorigenicity. Nat. Cell Biol. *13*, 1214–23.

S8. Delaval, B., Bright, A., Lawson, N. D., and Doxsey, S. (2011). The cilia protein IFT88 is required for spindle orientation in mitosis. Nat. Cell Biol. *13*, 461–8.

S9. Doxsey, S. J., Stein, P., Evans, L., Calarco, P. D., and Kirschner, M. (1994). Pericentrin, a highly conserved centrosome protein involved in microtubule organization. Cell *76*, 639–50.

S10. Soung, N.-K., Kang, Y. H., Kim, K., Kamijo, K., Yoon, H., Seong, Y.-S., Kuo, Y.-L., Miki, T., Kim, S. R., Kuriyama, R., et al. (2006). Requirement of hCenexin for proper mitotic functions of polo-like kinase 1 at the centrosomes. Mol. Cell. Biol. *26*, 8316–35.